

Observation of Resonance Structures in $e^+e^- \rightarrow \pi^+\pi^-\psi_2(3823)$ and Mass Measurement of $\psi_2(3823)$

M. Ablikim¹, M. N. Achasov^{10,b}, P. Adlarson⁶⁹, M. Albrecht⁴, R. Aliberti²⁹, A. Amoroso^{68A,68C}, M. R. An³³, Q. An^{65,51}, X. H. Bai⁵⁹, Y. Bai⁵⁰, O. Bakina³⁰, R. Baldini Ferroli^{24A}, I. Balossino^{25A}, Y. Ban^{40,g}, V. Batozskaya^{1,38}, D. Becker²⁹, K. Begzsuren²⁷, N. Berger²⁹, M. Bertani^{24A}, D. Bettoni^{25A}, F. Bianchi^{68A,68C}, J. Bloms⁶², A. Bortone^{68A,68C}, I. Boyko³⁰, R. A. Briere⁵, A. Brueggemann⁶², H. Cai⁷⁰, X. Cai^{1,51}, A. Calcaterra^{24A}, G. F. Cao^{1,56}, N. Cao^{1,56}, S. A. Cetin^{55A}, J. F. Chang^{1,51}, W. L. Chang^{1,56}, G. Chelkov^{30,a}, C. Chen³⁷, G. Chen¹, H. S. Chen^{1,56}, M. L. Chen^{1,51}, S. J. Chen³⁶, T. Chen¹, X. R. Chen^{26,56}, X. T. Chen¹, Y. B. Chen^{1,51}, Z. J. Chen^{21,h}, W. S. Cheng^{68C}, G. Cibinetto^{25A}, F. Cossio^{68C}, J. J. Cui⁴³, H. L. Dai^{1,51}, J. P. Dai⁷², A. Dbeyssi¹⁵, R. E. de Boer⁴, D. Dedovich³⁰, Z. Y. Deng¹, A. Denig²⁹, I. Denysenko³⁰, M. Destefanis^{68A,68C}, F. De Mori⁷², Y. Ding³⁴, J. Dong^{1,51}, L. Y. Dong^{1,56}, M. Y. Dong^{1,51,56}, X. Dong⁷⁰, S. X. Du⁷⁴, P. Egorov^{30,a}, Y. L. Fan⁷⁰, J. F. Fang^{1,51}, S. S. Fang^{1,56}, Y. Fang¹, R. Farinelli^{25A}, L. Fava^{68B,68C}, F. Feldbauer⁴, G. Felici^{24A}, C. Q. Feng^{65,51}, J. H. Feng⁵², K. Fischer⁶³, M. Fritsch⁴, C. D. Fu¹, H. Gao⁵⁶, Y. N. Gao^{40,g}, Yang Gao^{65,51}, S. Garbolino^{68C}, I. Garzia^{25A,25B}, P. T. Ge⁷⁰, Z. W. Ge³⁶, C. Geng⁵², E. M. Gersabeck⁶⁰, A. Gilman⁶³, K. Goetzen¹¹, L. Gong³⁴, W. X. Gong^{1,51}, W. Gradl²⁹, M. Greco^{68A,68C}, L. M. Gu³⁶, M. H. Gu^{1,51}, Y. T. Gu¹³, C. Y. Guan^{1,56}, A. Q. Guo^{26,56}, L. B. Guo³⁵, R. P. Guo⁴², Y. P. Guo^{9,f}, A. Guskov^{30,a}, T. T. Han⁴³, W. Y. Han³³, X. Q. Hao¹⁶, F. A. Harris⁵⁸, K. K. He⁴⁸, K. L. He^{1,56}, F. H. Heinsius⁴, C. H. Heinz²⁹, Y. K. Heng^{1,51,56}, C. Herold⁵³, M. Himmelreich^{11,d}, T. Holtmann⁴, G. Y. Hou^{1,56}, Y. R. Hou⁵⁶, Z. L. Hou¹, H. M. Hu^{1,56}, J. F. Hu^{49,i}, T. Hu^{1,51,56}, Y. Hu¹, G. S. Huang^{65,51}, K. X. Huang⁵², L. Q. Huang⁶⁶, L. Q. Huang^{26,56}, X. T. Huang⁴³, Y. P. Huang¹, Z. Huang^{40,g}, T. Hussain⁶⁷, N. Hüsken^{23,29}, W. Imoehl²³, M. Irshad^{65,51}, J. Jackson²³, S. Jaeger⁴, S. Janchiv²⁷, Q. Ji¹, Q. P. Ji¹⁶, X. B. Ji^{1,56}, X. L. Ji^{1,51}, Y. Y. Ji⁴³, Z. K. Jia^{65,51}, H. B. Jiang⁴³, S. S. Jiang³³, X. S. Jiang^{1,51,56}, Y. Jiang⁵⁶, J. B. Jiao⁴³, Z. Jiao¹⁹, S. Jin³⁶, Y. Jin⁵⁹, M. Q. Jing^{1,56}, T. Johansson⁶⁹, N. Kalantar-Nayestanaki⁵⁷, X. S. Kang³⁴, R. Kappert⁵⁷, M. Kavatsyuk⁵⁷, B. C. Ke⁷⁴, I. K. Keshk⁴, A. Khoukaz⁶², P. Kiese²⁹, R. Kiuchi¹, R. Kliemt¹¹, L. Koch³¹, O. B. Kolcu^{55A}, B. Kopf⁴, M. Kuemmel⁴, M. Kuessner⁴, A. Kupsc^{38,69}, W. Kühn³¹, J. J. Lane⁶⁰, J. S. Lange³¹, P. Larin¹⁵, A. Lavanian²², L. Lavezzi^{68A,68C}, Z. H. Lei^{65,51}, H. Leithoff^{62,9}, M. Lellmann²⁹, T. Lenz²⁹, C. Li⁴¹, C. Li³⁷, C. H. Li³³, Cheng Li^{65,51}, D. M. Li⁷⁴, F. Li^{1,51}, G. Li¹, H. Li^{65,51}, H. Li⁴⁵, H. B. Li^{1,56}, H. J. Li¹⁶, H. N. Li^{49,i}, J. Q. Li⁴, J. S. Li⁵², J. W. Li⁴³, Ke Li¹, L. J. Li¹, L. K. Li¹, Lei Li³, M. H. Li³⁷, P. R. Li^{32,j,k}, S. X. Li⁹, S. Y. Li⁵⁴, T. Li⁴³, W. D. Li^{1,56}, W. G. Li¹, X. H. Li^{65,51}, X. L. Li⁴³, Xiaoyu Li^{1,56}, Z. Y. Li⁵², H. Liang²⁸, H. Liang^{65,51}, H. Liang^{1,56}, Y. F. Liang⁴⁷, Y. T. Liang^{26,56}, G. R. Liao¹², L. Z. Liao⁴³, J. Libby²², A. Limphirat⁵³, C. X. Lin⁵², D. X. Lin^{26,56}, T. Lin¹, B. J. Liu¹, C. X. Liu¹, D. Liu^{15,65}, F. H. Liu⁴⁶, Fang Liu¹, Feng Liu⁶, G. M. Liu^{49,i}, H. B. Liu¹³, H. M. Liu^{1,56}, Huanhuan Liu¹, Huihui Liu¹⁷, J. B. Liu^{65,51}, J. L. Liu⁶⁶, J. Y. Liu^{1,56}, K. Liu¹, K. Y. Liu³⁴, Ke Liu¹⁸, L. Liu^{65,51}, Lu Liu³⁷, M. H. Liu^{9,f}, P. L. Liu¹, Q. Liu⁵⁶, S. B. Liu^{65,51}, T. Liu^{9,f}, W. K. Liu³⁷, W. M. Liu^{65,51}, X. Liu^{32,j,k}, Y. Liu^{32,j,k}, Y. B. Liu³⁷, Z. A. Liu^{1,51,56}, Z. Q. Liu⁴³, X. C. Lou^{1,51,56}, F. X. Lu⁵², H. J. Lu¹⁹, J. G. Lu^{1,51}, X. L. Lu¹, Y. Lu¹, Y. P. Lu^{1,51}, Z. H. Lu¹, C. L. Luo³⁵, M. X. Luo⁷³, T. Luo^{9,f}, X. L. Luo^{1,51}, X. R. Lyu⁵⁶, Y. F. Lyu³⁷, F. C. Ma³⁴, H. L. Ma¹, L. L. Ma⁴³, M. M. Ma^{1,56}, Q. M. Ma¹, R. Q. Ma^{1,56}, R. T. Ma⁵⁶, X. Y. Ma^{1,51}, Y. Ma^{40,g}, F. E. Maas¹⁵, M. Maggiora^{68A,68C}, S. Maldaner⁴, S. Malde⁶³, Q. A. Malik⁶⁷, A. Mangoni^{24B}, Y. J. Mao^{40,g}, Z. P. Mao¹, S. Marcello^{68A,68C}, Z. X. Meng⁵⁹, J. G. Messchendorp^{57,11}, G. Mezzadri^{25A}, H. Miao¹, T. J. Min³⁶, R. E. Mitchell²³, X. H. Mo^{1,51,56}, N. Yu. Muchnoi^{10,b}, H. Muramatsu⁶¹, S. Nakhoul^{11,d}, Y. Nefedov³⁰, F. Nerling^{11,d}, I. B. Nikolaev^{10,b}, Z. Ning^{1,51}, S. Nisar^{8,l}, Y. Niu⁴³, S. L. Olsen⁵⁶, Q. Ouyang^{1,51,56}, S. Pacetti^{24B,24C}, X. Pan^{9,f}, Y. Pan⁶⁰, A. Pathak²⁸, M. Pelizaeus⁴, H. P. Peng^{65,51}, K. Peters^{11,d}, J. L. Ping³⁵, R. G. Ping^{1,56}, S. Plura²⁹, S. Pogodin³⁰, R. Poling⁶¹, V. Prasad^{65,51}, H. Qi^{65,51}, H. R. Qi⁵⁴, M. Qi³⁶, T. Y. Qi^{9,f}, S. Qian^{1,51}, W. B. Qian⁵⁶, Z. Qian⁵², C. F. Qiao⁵⁶, J. J. Qin⁶⁶, L. Q. Qin¹², X. P. Qin^{9,f}, X. S. Qin⁴³, Z. H. Qin^{1,51}, J. F. Qiu¹, S. Q. Qu⁵⁴, K. H. Rashid⁶⁷, K. Ravindran²², C. F. Redmer²⁹, K. J. Ren³³, A. Rivetti^{68C}, V. Rodin⁵⁷, M. Rolo^{68C}, G. Rong^{1,56}, Ch. Rosner¹⁵, A. Sarantsev^{30,c}, Y. Schelhaas²⁹, C. Schmier⁴, K. Schoenning⁶⁹, M. Scodreggio^{25A,25B}, K. Y. Shan^{9,f}, W. Shan²⁰, X. Y. Shan^{65,51}, J. F. Shanguan⁴⁸, L. G. Shao^{1,56}, M. Shao^{65,51}, C. P. Shen^{9,f}, H. F. Shen^{1,56}, X. Y. Shen^{1,56}, B. A. Shi⁵⁶, H. C. Shi^{65,51}, R. S. Shi^{1,56}, X. Shi^{1,51}, X. D. Shi^{65,51}, J. J. Song¹⁶, W. M. Song^{28,1}, Y. X. Song^{40,g}, S. Sosio^{68A,68C}, S. Spataro^{68A,68C}, F. Stieler²⁹, K. X. Su⁷⁰, P. P. Su⁴⁸, Y. J. Su⁵⁶, G. X. Sun¹, H. Sun⁵⁶, H. K. Sun¹, J. F. Sun¹⁶, L. Sun⁷⁰, S. S. Sun^{1,56}, T. Sun^{1,56}, W. Y. Sun²⁸, X. Sun^{21,h}, Y. J. Sun^{65,51}, Y. Z. Sun¹, Z. T. Sun⁴³, Y. H. Tan⁷⁰, Y. X. Tan^{65,51}, C. J. Tang⁴⁷, G. Y. Tang¹, J. Tang⁵², L. Y. Tao⁶⁶, Q. T. Tao^{21,h}, J. X. Teng^{65,51}, V. Thoren⁶⁹, W. H. Tian⁴⁵, Y. Tian^{26,56}, I. Uman^{55B}, B. Wang¹, B. L. Wang⁵⁶, C. W. Wang³⁶, D. Y. Wang^{40,g}, F. Wang⁶⁶, H. J. Wang^{32,j,k}, H. P. Wang^{1,56}, K. Wang^{1,51}, L. L. Wang¹, M. Wang⁴³, M. Z. Wang^{40,g}, Meng Wang^{1,56}, S. Wang^{9,f}, S. Wang¹², T. Wang^{9,f}, T. J. Wang³⁷, W. Wang⁵², W. H. Wang⁷⁰, W. P. Wang^{65,51}, X. Wang^{40,g}, X. F. Wang^{32,j,k}, X. L. Wang^{9,f}, Y. D. Wang³⁹, Y. F. Wang^{1,51,56}, Y. H. Wang⁴¹, Y. Q. Wang¹, Z. Wang^{1,51}, Z. Y. Wang^{1,56}, Ziyi Wang⁵⁶, D. H. Wei¹², F. Weidner⁶², S. P. Wen¹, D. J. White⁶⁰, U. Wiedner⁴, G. Wilkinson⁶³, M. Wolke⁶⁹, L. Wollenberg¹, J. F. Wu^{1,56}, L. H. Wu¹, L. J. Wu^{1,56}, X. Wu^{9,f}, X. H. Wu²⁸, Y. Wu⁶⁵, Y. J. Wu²⁶, Z. Wu^{1,51}, L. Xia^{65,51}, T. Xiang^{40,g}, G. Y. Xiao³⁶, H. Xiao^{9,f}, S. Y. Xiao¹, Y. L. Xiao^{9,f}, Z. J. Xiao³⁵, C. Xie³⁶, X. H. Xie^{40,g}, Y. Xie⁴³, Y. G. Xie^{1,51}, Y. H. Xie⁶, Z. P. Xie^{65,51}, T. Y. Xing^{1,56}, C. F. Xu¹, C. J. Xu⁵², G. F. Xu¹, H. Y. Xu⁵⁹, Q. J. Xu¹⁴, X. P. Xu⁴⁸, Y. C. Xu⁵⁶, Z. P. Xu³⁶, F. Yan^{9,f}, L. Yan^{9,f}, W. B. Yan^{65,51}, W. C. Yan⁷⁴, H. J. Yang^{44,e}, H. L. Yang²⁸, H. X. Yang¹, L. Yang⁴⁵, S. L. Yang⁵⁶, Y. X. Yang^{1,56}, Yifan Yang^{1,56}, M. Ye^{1,51}, M. H. Ye⁷, J. H. Yin¹, Z. Y. You⁵², B. X. Yu^{1,51,56}, C. X. Yu³⁷, G. Yu^{1,56}, J. S. Yu^{21,h}, T. Yu⁶⁶, C. Z. Yuan^{1,56}, L. Yuan², S. C. Yuan¹, X. Q. Yuan¹, Y. Yuan^{1,56}, Z. Y. Yuan⁵², C. X. Yue³³, A. A. Zafar⁶⁷, F. R. Zeng⁴³, X. Zeng⁶, Y. Zeng^{21,h}, Y. H. Zhan⁵², A. Q. Zhang¹, B. L. Zhang¹, B. X. Zhang¹, G. Y. Zhang¹⁶, H. Zhang⁶⁵, H. H. Zhang⁵², H. H. Zhang²⁸, H. Y. Zhang^{1,51}, J. L. Zhang⁷¹, J. Q. Zhang³⁵, J. W. Zhang^{1,51,56}, J. Y. Zhang¹, J. Z. Zhang^{1,56}, Jianyu Zhang^{1,56}, Jiawei Zhang^{1,56}, L. M. Zhang⁵⁴, L. Q. Zhang⁵², Lei Zhang³⁶, P. Zhang¹, Q. Y. Zhang^{33,74}, Shuihan Zhang^{1,56}, Shulei Zhang^{21,h}, X. D. Zhang³⁹, X. M. Zhang¹, X. Y. Zhang⁴³, X. Y. Zhang⁴⁸, Y. Zhang⁶³, Y. T. Zhang⁷⁴, Y. H. Zhang^{1,51}, Yan Zhang^{65,51}, Yao Zhang¹, Z. H. Zhang¹, Z. Y. Zhang³⁷, Z. Y. Zhang⁷⁰, G. Zhao¹, J. Zhao³³, J. Y. Zhao^{1,51}, Lei Zhao^{65,51}, Ling Zhao¹, M. G. Zhao³⁷, Q. Zhao¹, S. J. Zhao⁷⁴, Y. B. Zhao^{1,51}, Y. X. Zhao^{26,56}, Z. G. Zhao^{65,51}, A. Zhemchugov^{30,a}, B. Zheng⁶⁶, J. P. Zheng^{1,51}, Y. H. Zheng⁵⁶, B. Zhong³⁵, C. Zhong⁶⁶, X. Zhong⁵², H. Zhou⁴³, L. P. Zhou^{1,56}, X. Zhou⁷⁰, X. K. Zhou⁵⁶, X. R. Zhou^{65,51}, X. Y. Zhou³³, Y. Z. Zhou^{9,f}, J. Zhu³⁷, K. Zhu¹, K. J. Zhu^{1,51,56}, L. X. Zhu⁵⁶, S. H. Zhu⁶⁴, S. Q. Zhu³⁶, T. J. Zhu⁷¹, W. J. Zhu^{9,f}, Y. C. Zhu^{65,51}, Z. A. Zhu^{1,56}, B. S. Zou¹, J. H. Zou¹

(BESIII Collaboration)

- ¹ Institute of High Energy Physics, Beijing 100049, People's Republic of China
- ² Beihang University, Beijing 100191, People's Republic of China
- ³ Beijing Institute of Petrochemical Technology, Beijing 102617, People's Republic of China
- ⁴ Bochum Ruhr-University, D-44780 Bochum, Germany
- ⁵ Carnegie Mellon University, Pittsburgh, Pennsylvania 15213, USA
- ⁶ Central China Normal University, Wuhan 430079, People's Republic of China
- ⁷ China Center of Advanced Science and Technology, Beijing 100190, People's Republic of China
- ⁸ COMSATS University Islamabad, Lahore Campus, Defence Road, Off Raiwind Road, 54000 Lahore, Pakistan
- ⁹ Fudan University, Shanghai 200433, People's Republic of China
- ¹⁰ G.I. Budker Institute of Nuclear Physics SB RAS (BINP), Novosibirsk 630090, Russia
- ¹¹ GSI Helmholtzcentre for Heavy Ion Research GmbH, D-64291 Darmstadt, Germany
- ¹² Guangxi Normal University, Guilin 541004, People's Republic of China
- ¹³ Guangxi University, Nanning 530004, People's Republic of China
- ¹⁴ Hangzhou Normal University, Hangzhou 310036, People's Republic of China
- ¹⁵ Helmholtz Institute Mainz, Staudinger Weg 18, D-55099 Mainz, Germany
- ¹⁶ Henan Normal University, Xinxiang 453007, People's Republic of China
- ¹⁷ Henan University of Science and Technology, Luoyang 471003, People's Republic of China
- ¹⁸ Henan University of Technology, Zhengzhou 450001, People's Republic of China
- ¹⁹ Huangshan College, Huangshan 245000, People's Republic of China
- ²⁰ Hunan Normal University, Changsha 410081, People's Republic of China
- ²¹ Hunan University, Changsha 410082, People's Republic of China
- ²² Indian Institute of Technology Madras, Chennai 600036, India
- ²³ Indiana University, Bloomington, Indiana 47405, USA
- ²⁴ INFN Laboratori Nazionali di Frascati, (A)INFN Laboratori Nazionali di Frascati, I-00044, Frascati, Italy; (B)INFN Sezione di Perugia, I-06100, Perugia, Italy; (C)University of Perugia, I-06100, Perugia, Italy
- ²⁵ INFN Sezione di Ferrara, (A)INFN Sezione di Ferrara, I-44122, Ferrara, Italy; (B)University of Ferrara, I-44122, Ferrara, Italy
- ²⁶ Institute of Modern Physics, Lanzhou 730000, People's Republic of China
- ²⁷ Institute of Physics and Technology, Peace Avenue 54B, Ulaanbaatar 13330, Mongolia
- ²⁸ Jilin University, Changchun 130012, People's Republic of China
- ²⁹ Johannes Gutenberg University of Mainz, Johann-Joachim-Becher-Weg 45, D-55099 Mainz, Germany
- ³⁰ Joint Institute for Nuclear Research, 141980 Dubna, Moscow region, Russia
- ³¹ Justus-Liebig-Universität Giessen, II. Physikalisches Institut, Heinrich-Buff-Ring 16, D-35392 Giessen, Germany
- ³² Lanzhou University, Lanzhou 730000, People's Republic of China
- ³³ Liaoning Normal University, Dalian 116029, People's Republic of China
- ³⁴ Liaoning University, Shenyang 110036, People's Republic of China
- ³⁵ Nanjing Normal University, Nanjing 210023, People's Republic of China
- ³⁶ Nanjing University, Nanjing 210093, People's Republic of China
- ³⁷ Nankai University, Tianjin 300071, People's Republic of China
- ³⁸ National Centre for Nuclear Research, Warsaw 02-093, Poland
- ³⁹ North China Electric Power University, Beijing 102206, People's Republic of China
- ⁴⁰ Peking University, Beijing 100871, People's Republic of China
- ⁴¹ Qufu Normal University, Qufu 273165, People's Republic of China
- ⁴² Shandong Normal University, Jinan 250014, People's Republic of China
- ⁴³ Shandong University, Jinan 250100, People's Republic of China
- ⁴⁴ Shanghai Jiao Tong University, Shanghai 200240, People's Republic of China
- ⁴⁵ Shanxi Normal University, Linfen 041004, People's Republic of China
- ⁴⁶ Shanxi University, Taiyuan 030006, People's Republic of China
- ⁴⁷ Sichuan University, Chengdu 610064, People's Republic of China
- ⁴⁸ Soochow University, Suzhou 215006, People's Republic of China
- ⁴⁹ South China Normal University, Guangzhou 510006, People's Republic of China
- ⁵⁰ Southeast University, Nanjing 211100, People's Republic of China
- ⁵¹ State Key Laboratory of Particle Detection and Electronics, Beijing 100049, Hefei 230026, People's Republic of China
- ⁵² Sun Yat-Sen University, Guangzhou 510275, People's Republic of China
- ⁵³ Suranaree University of Technology, University Avenue 111, Nakhon Ratchasima 30000, Thailand
- ⁵⁴ Tsinghua University, Beijing 100084, People's Republic of China
- ⁵⁵ Turkish Accelerator Center Particle Factory Group, (A)Istinye University, 34010, Istanbul, Turkey; (B)Near East University, Nicosia, North Cyprus, Mersin 10, Turkey
- ⁵⁶ University of Chinese Academy of Sciences, Beijing 100049, People's Republic of China
- ⁵⁷ University of Groningen, NL-9747 AA Groningen, The Netherlands
- ⁵⁸ University of Hawaii, Honolulu, Hawaii 96822, USA
- ⁵⁹ University of Jinan, Jinan 250022, People's Republic of China
- ⁶⁰ University of Manchester, Oxford Road, Manchester, M13 9PL, United Kingdom
- ⁶¹ University of Minnesota, Minneapolis, Minnesota 55455, USA
- ⁶² University of Muenster, Wilhelm-Klemm-Strasse 9, 48149 Muenster, Germany

⁶³ *University of Oxford, Keble Road, Oxford OX13RH, United Kingdom*

⁶⁴ *University of Science and Technology Liaoning, Anshan 114051, People's Republic of China*

⁶⁵ *University of Science and Technology of China, Hefei 230026, People's Republic of China*

⁶⁶ *University of South China, Hengyang 421001, People's Republic of China*

⁶⁷ *University of the Punjab, Lahore-54590, Pakistan*

⁶⁸ *University of Turin and INFN, (A)University of Turin, I-10125, Turin, Italy; (B)University of Eastern Piedmont, I-15121, Alessandria, Italy; (C)INFN, I-10125, Turin, Italy*

⁶⁹ *Uppsala University, Box 516, SE-75120 Uppsala, Sweden*

⁷⁰ *Wuhan University, Wuhan 430072, People's Republic of China*

⁷¹ *Xinyang Normal University, Xinyang 464000, People's Republic of China*

⁷² *Yunnan University, Kunming 650500, People's Republic of China*

⁷³ *Zhejiang University, Hangzhou 310027, People's Republic of China*

⁷⁴ *Zhengzhou University, Zhengzhou 450001, People's Republic of China*

^a *Also at the Moscow Institute of Physics and Technology, Moscow 141700, Russia*

^b *Also at the Novosibirsk State University, Novosibirsk, 630090, Russia*

^c *Also at the NRC "Kurchatov Institute", PNPI, 188300, Gatchina, Russia*

^d *Also at Goethe University Frankfurt, 60323 Frankfurt am Main, Germany*

^e *Also at Key Laboratory for Particle Physics, Astrophysics and Cosmology, Ministry of Education; Shanghai Key Laboratory for Particle Physics and Cosmology; Institute of Nuclear and Particle Physics, Shanghai 200240, People's Republic of China*

^f *Also at Key Laboratory of Nuclear Physics and Ion-beam Application (MOE) and Institute of Modern Physics, Fudan University, Shanghai 200443, People's Republic of China*

^g *Also at State Key Laboratory of Nuclear Physics and Technology, Peking University, Beijing 100871, People's Republic of China*

^h *Also at School of Physics and Electronics, Hunan University, Changsha 410082, China*

ⁱ *Also at Guangdong Provincial Key Laboratory of Nuclear Science, Institute of Quantum Matter, South China Normal University, Guangzhou 510006, China*

^j *Also at Frontiers Science Center for Rare Isotopes, Lanzhou University, Lanzhou 730000, People's Republic of China*

^k *Also at Lanzhou Center for Theoretical Physics, Lanzhou University, Lanzhou 730000, People's Republic of China*

^l *Also at the Department of Mathematical Sciences, IBA, Karachi, Pakistan*

(Dated: September 7, 2022)

Using a data sample corresponding to an integrated luminosity of 11.3 fb^{-1} collected at center-of-mass energies from 4.23 to 4.70 GeV with the BESIII detector, we measure the product of the $e^+e^- \rightarrow \pi^+\pi^-\psi_2(3823)$ cross section and the branching fraction $\mathcal{B}[\psi_2(3823) \rightarrow \gamma\chi_{c1}]$. For the first time, resonance structure is observed in the cross section line shape of $e^+e^- \rightarrow \pi^+\pi^-\psi_2(3823)$ with significances exceeding 5σ . A fit to data with two coherent Breit-Wigner resonances modeling the \sqrt{s} -dependent cross section yields $M(R_1) = 4406.9 \pm 17.2 \pm 4.5 \text{ MeV}/c^2$, $\Gamma(R_1) = 128.1 \pm 37.2 \pm 2.3 \text{ MeV}$, and $M(R_2) = 4647.9 \pm 8.6 \pm 0.8 \text{ MeV}/c^2$, $\Gamma(R_2) = 33.1 \pm 18.6 \pm 4.1 \text{ MeV}$. Though weakly disfavored by the data, a single resonance with $M(R) = 4417.5 \pm 26.2 \pm 3.5 \text{ MeV}/c^2$, $\Gamma(R) = 245 \pm 48 \pm 13 \text{ MeV}$ is also possible to interpret data. This observation deepens our understanding of the nature of the vector charmoniumlike states. The mass of the $\psi_2(3823)$ state is measured as $(3823.12 \pm 0.43 \pm 0.13) \text{ MeV}/c^2$, which is the most precise measurement to date.

PACS numbers: 13.20.Gd, 13.25.Gv, 14.40.Pq

In the quark model, hadrons are strongly-interacting, composite particles built from colour-neutral combinations of quarks and antiquarks [1]. It was long thought that all observed hadrons fall into two classes only: baryons, composed of three quarks, and mesons, bound states of a quark-antiquark pair. The QCD theory describing the strong interaction also allowed for other colour-neutral configurations, but there was no experimental evidence for such ‘exotic’ hadrons.

This simple picture, however, has been challenged since 2003, when many new charmonium-like states such as the $\chi_{c1}(3872)$ [2], $\psi(4260)$ [3], and $Z_c(3900)$ [4, 5] have been observed experimentally. These particles can not easily be accommodated in the spectrum of conventional charmonium states and are widely considered to be promising candidates for QCD exotic hadrons [6, 7]. Among them, the vector ψ -states usually couple to hidden charm final states like J/ψ , $\psi(2S)$, or h_c via dipion transitions, such as the $\psi(4260) \rightarrow$

$\pi^+\pi^-J/\psi$ [3, 8, 9], $\psi(4360)/\psi(4660) \rightarrow \pi^+\pi^-\psi(2S)$ [10, 11], and $\psi(4390) \rightarrow \pi^+\pi^-h_c$ [12]. In addition, there are also vector states with mass above 4.6 GeV reported in $e^+e^- \rightarrow \Lambda_c^+\Lambda_c^-$ [13], and $e^+e^- \rightarrow D_s^+D_{s1}(2536)^-/D_s^+D_{s2}^*(2573)^-$ processes [14]. At the moment, experimental information about these ψ -states, especially for the high mass states is still quite limited. It is not clear whether $\psi(4360)$ and $\psi(4390)$ correspond to the same resonance or not. Above 4.6 GeV, the resonance parameters of vector states observed in hidden-charm and open-charm final states are not exactly the same. Whether there exists one or more resonances is a long-standing puzzle in the study of the vector charmonium-like spectrum. To pin down these issues, new observations from experiment are urgently needed.

One of the vector states, the $\psi(4660)$ resonance, was first observed by the Belle experiment [11] and later confirmed by the BABAR and BESIII experiments [15, 16]. It remains,

however, unclear what the exact nature is of the $\psi(4660)$. Possible interpretations of its internal structure include a hadronic molecule [17], a baryonium [18], or a compact tetraquark state [19]. For these theoretical models, the coupling of $\psi(4660)$ to the $\psi(2S)$ state with no or weak coupling to other charmonium states is an essential element. Therefore, a search for the decay of $\psi(4660)$ to final state other than $\psi(2S)$ in experiment helps to test various pictures for the $\psi(4660)$ structure.

The D -wave charmonium state $\psi_2(3823)$ [20, 21] and $\psi_3(3842)$ [22] were well established recently, and several decay modes of the $\psi_2(3823)$ state are also observed [23]. It serves as a new probe to study the vector ψ -states. We search for the dipion transition of $\psi(4660)$ to $\psi_2(3823)$, which on the one hand helps establish the $\psi(4660)$ state, on the other hand sheds light on its internal structure. At the same time, the $\psi_2(3823)$ mass is also precisely measured, which can be used to calibrate the parameters in the potential model [24], and finally greatly deepens our understanding of the dynamics of the $c\bar{c}$ system.

In this Letter, we measure the \sqrt{s} -dependent production cross section of the process $e^+e^- \rightarrow \pi^+\pi^-\psi_2(3823)$, and explore the resonance structures in the cross section line shape. The resonance parameters of the $\psi_2(3823)$ state are measured as well. To increase the yield of signal events, a partial reconstruction approach is employed. We use a data sample corresponding to an integrated luminosity of 11.3 fb^{-1} , taken at center-of-mass (c.m.) energies from $\sqrt{s} = 4.23$ to 4.70 GeV [25], with the BESIII detector [26] operating at the BEPCII storage ring [27]. The $\psi_2(3823)$ candidates are reconstructed in their $\gamma\chi_{c1}$ decay mode, with $\chi_{c1} \rightarrow \gamma J/\psi$ and $J/\psi \rightarrow \ell^+\ell^-$ ($\ell = e$ or μ).

The BESIII detector is described in detail elsewhere [26, 28]. A GEANT4-based [29] Monte Carlo (MC) simulation software package is used to optimize event selection criteria, determine the detection efficiency, and estimate the backgrounds. For the signal process, we generate 50,000 $e^+e^- \rightarrow \pi^+\pi^-\psi_2(3823)$ events at each c.m. energy using an EVTGEN [30] phase space model. Initial-state-radiation (ISR) is simulated with KKMC [31], where we use the $e^+e^- \rightarrow \pi^+\pi^-\psi_2(3823)$ cross section measured from this analysis as input. The maximum ISR photon energy is set to correspond to the production threshold of the $\pi^+\pi^-\psi_2(3823)$ system at $4.1 \text{ GeV}/c^2$. Final-state-radiation is simulated with PHOTOS [32].

Events with four good charged tracks with net charge zero are selected as described in Ref. [21]. Electromagnetic showers identified as photon candidates must satisfy fiducial shower quality as well as timing requirements as described in Ref. [33]. For events with only one photon candidate ($N_\gamma = 1$), assuming that only one of the two radiative photons is detected, we use a partial reconstruction strategy, *i.e.* allowing one missing photon (γ_{miss}). The mass square of the missing photon candidate is required to be $-0.07 < M_{\text{miss}}^2(\gamma) < 0.08 \text{ GeV}^2/c^4$ (with a signal efficiency $> 99\%$), where the 4-momentum of γ_{miss} is computed from momentum conservation. To improve the momentum and energy resolution and

to further reduce background, a one-constraint (1C) kinematic fit is performed under the hypothesis of $\pi^+\pi^-\ell^+\ell^-\gamma\gamma_{\text{miss}}$ to the initial e^+e^- c.m. system. The χ^2/ndf of the kinematic fit is required to be less than 15/1. For multi-photon events ($N_\gamma \geq 2$), we use the full reconstruction strategy as described in Ref. [21].

To reject radiative Bhabha and radiative dimuon ($\gamma e^+e^-/\gamma\mu^+\mu^-$) background events with gamma-conversion ($\gamma \rightarrow e^+e^-$), where the converted electrons are misidentified as pions, the cosine of the opening angle of the pion pairs is required to be less than 0.98. The background from $e^+e^- \rightarrow \eta J/\psi$ with $\eta \rightarrow \pi^+\pi^-\pi^0/\gamma\pi^+\pi^-$ is effectively rejected by the invariant mass requirement $M(\gamma\gamma_{\text{miss}}\pi^+\pi^-) > 0.65 \text{ GeV}/c^2$. In order to remove possible backgrounds from $e^+e^- \rightarrow \gamma_{\text{ISR}}\psi(2S)$, $e^+e^- \rightarrow \eta\psi(2S)$ with $\eta \rightarrow \gamma\gamma$, and $e^+e^- \rightarrow \gamma\gamma\psi(2S)$ processes, the invariant mass of $\pi^+\pi^-J/\psi$ is required to satisfy $|M(\pi^+\pi^-J/\psi) - m[\psi(2S)]| > 7 \text{ MeV}/c^2$ [34].

According to a resolution of $(14.2 \pm 0.5) \text{ MeV}$ from $\psi(2S)$ data events for the $M(\ell^+\ell^-)$ mass, the J/ψ signal region is defined as $3.06 < M(\ell^+\ell^-) < 3.135 \text{ GeV}/c^2$. To estimate non- J/ψ backgrounds, we also define J/ψ mass sidebands as $2.950 < M(\ell^+\ell^-) < 3.025 \text{ GeV}/c^2$ or $3.170 < M(\ell^+\ell^-) < 3.245 \text{ GeV}/c^2$. To reconstruct the χ_{c1} candidate from the $\psi_2(3823)$ decay, the 4-momenta of the two radiative photons after the 1C kinematic fit are boosted to the c.m. frame of the $\psi_2(3823)$ system. The photon with the higher energy is used to reconstruct χ_{c1} , while the lower-energy one is considered to originate from the $\psi_2(3823)$ decay. MC simulation shows that the mis-assignment of the two photons is negligibly small ($< 1\%$). The mass window of the reconstructed χ_{c1} candidates is defined as $3.48 < M(\gamma_H J/\psi) < 3.53 \text{ GeV}/c^2$ [34], with a signal efficiency of 96%.

The possible remaining backgrounds mainly come from $e^+e^- \rightarrow (\eta'/\gamma\omega)J/\psi$, with $(\eta'/\omega) \rightarrow \gamma\gamma\pi^+\pi^-/\gamma\pi^+\pi^-$, and $\pi^+\pi^-\pi^+\pi^-(\pi^0/\gamma\gamma)$. The $e^+e^- \rightarrow (\eta'/\gamma\omega)J/\psi$ backgrounds are measured by BESIII using the same data set [35, 36] and can be reliably simulated. The $e^+e^- \rightarrow \pi^+\pi^-\pi^+\pi^-(\pi^0/\gamma\gamma)$ continuum background can be estimated by data in the J/ψ mass sidebands. All these background sources are found to be small, and only produce flat distributions in the $\psi_2(3823)$ signal region.

To achieve better sensitivity, the one-photon events (partial reconstruction) and the multi-photon events (full reconstruction) are separated. Figure 1 shows the $M^{\text{recoil}}(\pi^+\pi^-)$ distributions for data, where obvious $\psi(2S)$ and $\psi_2(3823)$ signal peaks are observed in both the one-photon and multi-photon events. Here, $M^{\text{recoil}}(\pi^+\pi^-) = \sqrt{(P_{e^+e^-} - P_{\pi^+} - P_{\pi^-})^2}$ is the recoil mass of $\pi^+\pi^-$, where $P_{e^+e^-}$ and P_{π^\pm} are the 4-momenta of the initial e^+e^- system and the reconstructed π^\pm candidates, respectively. For this expression, we use the π^\pm momenta without the kinematic fit correction because of the good resolution for low momentum pions according to MC simulation studies. A simultaneous unbinned extended maximum likelihood fit to the two $M^{\text{recoil}}(\pi^+\pi^-)$ distributions is performed to determine the parameters of the $\psi_2(3823)$ state. In the fit, the signal probability density function (PDF)

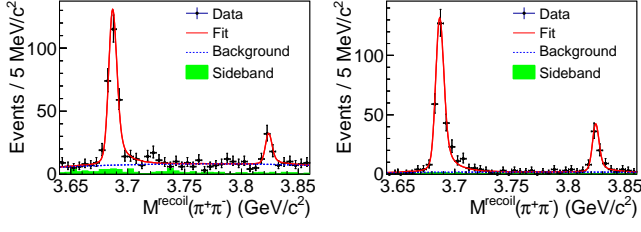


FIG. 1. Result of the simultaneous fit to the $M^{\text{recoil}}(\pi^+\pi^-)$ distributions for one-photon events (left) and multi-photon events (right). Dots with error bars are the selected data, the red solid curves are fit results, the blue dashed curves are backgrounds, and the green shaded histograms are backgrounds estimated from J/ψ mass sideband events.

is represented by $\psi(2S)$ and $\psi_2(3823)$ (with input mass of $3.823 \text{ GeV}/c^2$ and a zero natural width) MC simulated shapes, convolved with Gaussian functions with free mean μ and width σ to account for the mass and resolution difference between data and MC simulation, respectively. The background shape is parameterized as a second-order polynomial.

The fit results, also shown in Fig. 1, yield $M[\psi_2(3823)] = M[\psi_2(3823)]_{\text{input}} + \mu_{\psi_2(3823)} - \mu_{\psi(2S)} = 3823.12 \pm 0.43 \text{ MeV}/c^2$, where $M[\psi_2(3823)]_{\text{input}}$ is the input $\psi_2(3823)$ mass in MC simulation; $\mu_{\psi_2(3823)} = 1.02 \pm 0.43 \text{ MeV}/c^2$ and $\mu_{\psi(2S)} = 0.90 \pm 0.22 \text{ MeV}/c^2$ are the mass shift values for the $\psi_2(3823)$ and $\psi(2S)$ shapes, respectively. The total number of $\psi_2(3823)$ signal events determined from the fit is 120.0 ± 13.6 . The statistical significance of the $\psi_2(3823)$ signal is estimated to be 13.4σ , by comparing the difference between the log-likelihood value [$\Delta(\ln \mathcal{L}) = 96.6$] with or without the $\psi_2(3823)$ signal in the fit and taking the change of the number of degrees of freedom ($\Delta\text{ndf} = 4$) into account. We are not able to measure the intrinsic width of $\psi_2(3823)$ precisely because of the limited data sample size. From a fit using a Breit-Wigner (BW) function (with a width parameter that is left free) convolved with a double Gaussian function as signal PDF for $\psi_2(3823)$, we set an upper limit of $\Gamma[\psi_2(3823)] < 2.9 \text{ MeV}$ at the 90% confidence level (C.L.).

The product of the \sqrt{s} -dependent $e^+e^- \rightarrow \pi^+\pi^-\psi_2(3823)$ cross section and the branching ratio of $\psi_2(3823) \rightarrow \gamma\chi_{c1}$ is calculated as $\sigma[e^+e^- \rightarrow \pi^+\pi^-\psi_2(3823)] \cdot \mathcal{B}[\psi_2(3823) \rightarrow \gamma\chi_{c1}] = \frac{N^{\text{sig}}}{\mathcal{L}_{\text{int}} \epsilon \mathcal{B}(1+\delta)}$, where N^{sig} is the number of $\psi_2(3823) \rightarrow \gamma\chi_{c1}$ signal events obtained from a same fit (σ fixed to previous result) to the $M^{\text{recoil}}(\pi^+\pi^-)$ distribution at a certain c.m. energy, \mathcal{L}_{int} is the integrated luminosity, ϵ is the detection efficiency, \mathcal{B} is the branching fraction of $\chi_{c1} \rightarrow \gamma J/\psi \rightarrow \gamma \ell^+\ell^-$, and $(1+\delta)$ is the radiative correction factor, which depends on the cross section line shape of $e^+e^- \rightarrow \pi^+\pi^-\psi_2(3823)$. Since visible enhancements are observed near 4.40 and 4.65 GeV in the cross section line shape, the radiative correction factors are first obtained by modelling the line shape with two coherent BW resonances, and then iterated by updating the cross section measurement until this procedure converges, with

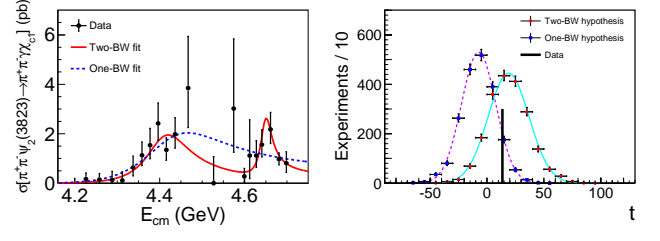


FIG. 2. (Left panel) result of the fit to the \sqrt{s} -dependent cross section $\sigma[e^+e^- \rightarrow \pi^+\pi^-\psi_2(3823)]$ times the branching ratio $\mathcal{B}[\psi_2(3823) \rightarrow \gamma\chi_{c1}]$. Dots with error bars are data, and the red solid (blue dashed) curve shows the fit with two coherent resonances (one resonance); (right panel) the likelihood ratio $t = -2 \ln \frac{\mathcal{L}_{1\text{BW}}}{\mathcal{L}_{2\text{BW}}}$ distribution from MC pseudo-experiments under two cross section hypothesis. Red dots (blue squares) with error bars are the two resonances (one resonance) hypothesis, and the black line shows data measurement.

a relative difference for $(1+\delta)\epsilon < 1\%$ between the last two iterations. The numerical results of the cross section measurement are listed in the supplemental material [37].

To extract the resonance structures in $\sigma[e^+e^- \rightarrow \pi^+\pi^-\psi_2(3823)]$, a maximum likelihood fit using the coherent sum of two BW resonances to model the measured cross section is performed to data events in the $\psi_2(3823)$ signal interval $[3.815, 3.835] \text{ GeV}/c^2$. The likelihood is constructed as that in Ref. [38]. There are two solutions with identical fit quality, and all resonance parameters from the fit are summarized in Table I. In addition, a fit with one single BW resonance to model the cross section yields $M[R] = 4417.5 \pm 26.2 \text{ MeV}/c^2$, $\Gamma_{\text{tot}}[R] = 245 \pm 48 \text{ MeV}$, $\Gamma_{e^+e^-} \mathcal{B}_1 \mathcal{B}_2 = 0.57 \pm 0.08 \text{ eV}/c^2$. The fit result is shown in Fig. 2. To discriminate the two resonances hypothesis (H_1) from the one resonance hypothesis (H_0) for the cross section interpretation, the likelihood ratio $t = -2 \ln \frac{\mathcal{L}_{1\text{BW}}}{\mathcal{L}_{2\text{BW}}}$ is used as a test variable. We perform 2000 MC pseudo-experiments for both hypotheses and the corresponding t -distributions are shown in Fig. 2. The $t = 13.6$ from data is positive and slightly favors H_1 . The p -value to reject H_0 is 8.2%, corresponding to a significance of 1.7σ . Other possible continuum parametrizations of the cross section in the fit, such as a shape of three-body phase space, $1/s^n$, or a product of phase space with $1/s^n$ are also tested, and they are not able to describe data well. The significance for the resonance hypothesis (with either one or two resonances) over continuum is estimated to be greater than 5σ .

The systematic uncertainties in the $\psi_2(3823)$ mass measurement include those from the absolute mass scale, resolution, parameterization of the $\psi_2(3823)$ signal and background shapes. In the $\psi_2(3823)$ mass measurement, we use the $\psi(2S)$ mass to calibrate the absolute mass scale. The uncertainty from the $\psi(2S)$ mass measurement is therefore taken as the systematic uncertainty due to the absolute mass scale, which is $0.12 \text{ MeV}/c^2$. To increase the $\psi(2S)$ sample size and thus reduce the $\psi(2S)$ mass uncertainty, we also employ $\psi(2S) \rightarrow \gamma\chi_{c2}$ and $\psi(2S) \rightarrow \eta J/\psi$ data events. The resolution difference between data and MC simulation is also es-

TABLE I. Results of the fit to the distribution of $\sigma[e^+e^- \rightarrow \pi^+\pi^-\psi_2(3823)] \cdot \mathcal{B}[\psi_2(3823) \rightarrow \gamma\chi_{c1}]$ with two coherent resonances. Here, $M[R_i]$ and $\Gamma_{\text{tot}}[R_i]$ represent the mass (in MeV/ c^2) and total width (in MeV) of resonance R_i , respectively; $\Gamma_{e^+e^-}\mathcal{B}_1^{R_i}\mathcal{B}_2$ is the product of the e^+e^- partial width (in eV/ c^2) and branching fraction of $R_i \rightarrow \pi^+\pi^-\psi_2(3823) \rightarrow \pi^+\pi^-\gamma\chi_{c1}$ ($i = 1, 2$). The parameter ϕ (in degrees) is the relative phase between the two resonances. The first uncertainties are statistical and the second systematic.

Parameters	Solution I	Solution II
$M[R_1]$	$4406.9 \pm 17.2 \pm 4.5$	
$\Gamma_{\text{tot}}[R_1]$	$128.1 \pm 37.2 \pm 2.3$	
$\Gamma_{e^+e^-}\mathcal{B}_1^{R_1}\mathcal{B}_2$	$0.36 \pm 0.10 \pm 0.03$	$0.30 \pm 0.09 \pm 0.03$
$M[R_2]$	$4647.9 \pm 8.6 \pm 0.8$	
$\Gamma_{\text{tot}}[R_2]$	$33.1 \pm 18.6 \pm 4.1$	
$\Gamma_{e^+e^-}\mathcal{B}_1^{R_2}\mathcal{B}_2$	$0.24 \pm 0.07 \pm 0.02$	$0.06 \pm 0.03 \pm 0.01$
ϕ	$267.1 \pm 16.2 \pm 3.2$	$-324.8 \pm 43.0 \pm 5.7$

estimated using the $\psi(2S)$ events. Fixing the resolution from a free value to the one measured with $\psi(2S)$ events, the mass difference for $\psi_2(3823)$ in the fit is 0.01 MeV/ c^2 . In the nominal fit, the signal PDF of $\psi_2(3823)$ is parameterized as a MC simulated shape convolved with Gaussian resolution. A signal PDF parameterized as a BW convolved with Gaussian resolution is also tested, and the mass difference (0.03 MeV/ c^2) is taken as the systematic uncertainty from signal parameterization. Changing the background shape from a second-order polynomial to a linear term yields 0.03 MeV/ c^2 mass difference associated with the background shape parameterization. Assuming that all the sources are independent, the total systematic uncertainty is calculated by adding them in quadrature, resulting in 0.13 MeV/ c^2 for the $\psi_2(3823)$ mass measurement. For the $\psi_2(3823)$ width, we measure the upper limits with all of the above systematic uncertainty sources, and report the most conservative one.

The systematic uncertainties in the cross section measurement mainly come from luminosity measurement, efficiencies, kinematic fit, signal shape, background shape, decay model, radiative correction, branching ratios and MC sample size. The luminosity is measured using Bhabha events, with an uncertainty of 1.0% [25]. The uncertainty in the tracking efficiency for high momentum leptons is 1.0% per track. Pions have momenta between 0.1 and 0.6 GeV/ c , and the momentum-weighted uncertainty is 1.0% per track. By requiring at least one good photon candidate to be detected, the photon detection efficiency is very high and the uncertainty is negligible. The systematic uncertainty for the choice of J/ψ mass window is similar to that of Ref. [39], which is 1.6%. A track helix parameters correction method as discussed in Ref. [40] is applied to each MC simulated event during the 1C kinematic fit. The difference in detection efficiencies with or without corrections, 1.7%, is assigned as the systematic uncertainty from kinematic fit. The same sources of signal and background shape parameterizations as discussed for the $\psi_2(3823)$ mass measurement would contribute 3.9%

and 1.4% differences in the $\psi_2(3823)$ signal events yields, which are taken as systematic uncertainties in the cross section measurement. We model the $e^+e^- \rightarrow \pi^+\pi^-\psi_2(3823)$ process with $L = 2$ between $\pi^+\pi^-$ and $\psi_2(3823)$ in the MC simulation. The efficiency difference between this model and a three-body phase space model is 1.8%. For the radiative correction, we take an alternative cross section line shape from one BW resonance model, and the difference for $(1 + \delta)\epsilon$ to the nominal two BW resonances model is 5.0%. The uncertainties on the branching ratios for $\chi_{c1} \rightarrow \gamma J/\psi$ (2.9%) and $J/\psi \rightarrow \ell^+\ell^-$ (0.5%) are taken from PDG [41]. The uncertainty from MC sample size is 0.6%. Assuming that all the sources are independent, the total systematic uncertainty is calculated by adding them in quadrature, resulting in 8.8% for the cross section measurement.

The systematic uncertainties for the resonance parameters in the cross section fit come from absolute c.m. energy measurement, the cross section uncertainty, and the fit model. The c.m. energies of data sets taken in different time periods are measured with different methods. Shifting the c.m. energies of data sets taken in the same period globally (*i. e.* fully correlated) within uncertainties, we repeat the cross section fit. The deviations of the resonance parameters are taken as systematic uncertainties. The systematic uncertainties on the cross section measurements are common to all c.m. energies and are propagated to $\Gamma_{e^+e^-}\mathcal{B}_1\mathcal{B}_2$ with the same amount. We quote 8.8% systematic uncertainty for $\Gamma_{e^+e^-}\mathcal{B}_1\mathcal{B}_2$. BW functions with constant full widths are used as the PDF in the cross section fit. We also use BW functions with \sqrt{s} -dependent full widths as the fit PDF, and the deviations of the resonance parameters between this fit and the nominal one are taken as systematic uncertainties from fit model. All these systematic contributions are listed in the supplemental material [37]. Assuming all the sources are independent, the total systematic uncertainties are calculated by adding them in quadrature.

In summary, the product of the $e^+e^- \rightarrow \pi^+\pi^-\psi_2(3823)$ cross section and the branching ratio of $\psi_2(3823) \rightarrow \gamma\chi_{c1}$, is measured with 11.3 fb $^{-1}$ data collected with the BESIII detector at $\sqrt{s} = 4.23$ to 4.70 GeV. For the first time, we observe resonance structure in the cross section line shape with a significance greater than 5σ . A fit to data with a sum of two coherent BW resonances to model the cross section yields the masses and widths of both resonances as shown in Tab. I. Although weakly disfavored by data with 1.7σ , a single resonance with a mass $4417.5 \pm 26.2 \pm 3.5$ MeV/ c^2 , and a width $245 \pm 48 \pm 13$ MeV is also possible to interpret data. Such a resonance has not been observed before. This is the first observation of vector ψ -states decaying to D -wave charmonium state, which provides new insights about the ψ -states wave functions. Considering that the measured $e^+e^- \rightarrow \pi^+\pi^-\psi(3770)$ cross section is also relatively large near 4.4 GeV [42], this indicates that the coupling between the ψ -states and D -wave charmonium might be popular, which should be taken into account when explaining the nature of these ψ -states.

Within current uncertainties, the parameters of structures in the two resonances interpretation are similar to the $\psi(4360)$ and $\psi(4660)$ states reported in $\pi^+\pi^-\psi(2S)$ [10, 11]. As-

suming the observed structures correspond to these resonances, this will be the second decay channel of the mysterious $\psi(4660)$ state after more than 15 years of discovery. By comparing the measured cross section of $\sigma[e^+e^- \rightarrow \pi^+\pi^-\psi_2(3823)]$ and $\sigma[e^+e^- \rightarrow \pi^+\pi^-\psi(2S)]$ [16], we find $\frac{\mathcal{B}[\psi(4660) \rightarrow \pi^+\pi^-\psi_2(3823)] \cdot \mathcal{B}[\psi_2(3823) \rightarrow \gamma\chi_{c1}]}{\mathcal{B}[\psi(4660) \rightarrow \pi^+\pi^-\psi(2S)]}$ reaches 10% level. Taking the branching fraction of $\mathcal{B}[\psi_2(3823) \rightarrow \gamma\chi_{c1}] \sim 50\%$ [43] as input, we obtain the relative partial decay width $\frac{\Gamma[\psi(4660) \rightarrow \pi^+\pi^-\psi_2(3823)]}{\Gamma[\psi(4660) \rightarrow \pi^+\pi^-\psi(2S)]} \sim 20\%$. This sizeable partial width poses a challenge to the $f_0(980)\psi(2S)$ hadron molecule interpretation [17] for the $\psi(4660)$ nature, which expects $\psi(4660)$ predominantly decaying into $f_0(980)\psi(2S)$. The observed $\psi(4660) \rightarrow \pi^+\pi^-\psi_2(3823)$ decay also differs from an extended baryonium picture [18] which explains the $\psi(4660)$ as a $\Sigma_c^0\bar{\Sigma}_c^0$ baryonium and speculates $\psi(4660)$ is a first radial excitation in accordance with the $n = 2$ radial quantum number of $\psi(2S)$ and absent coupling to charmonium states with $n = 1$. A similar argument also appears in a diquark-antidiquark tetraquark explanation [19], which assigns the $\psi(4660)$ as the radial excitation of the $\psi(4260)$ (a P -wave tetraquark) based on the only observed decay $\psi(4660) \rightarrow \pi^+\pi^-\psi(2S)$. Our observation obviously deviates from this assignment.

We also measure the mass of the $\psi_2(3823)$ state as $M[\psi_2(3823)] = 3823.12 \pm 0.43 \pm 0.13 \text{ MeV}/c^2$, where the first uncertainty is statistical and the second systematic. The $\psi_2(3823)$ width is studied, and an upper limit $\Gamma[\psi_2(3823)] < 2.9 \text{ MeV}$ at the 90% C.L. is obtained. This is the most precise measurement of the $\psi_2(3823)$ mass and the most stringent constraint on its width to date, which will help to refine the parameters of potential models and significantly reduce the uncertainties (ca. $\pm 50 \text{ MeV}$) of the D -wave states predicted

by the potential model [24].

The BESIII collaboration thanks the staff of BEPCII and the IHEP computing center for their strong support. This work is supported in part by National Key R&D Program of China under Contracts Nos. 2020YFA0406300, 2020YFA0406400; National Natural Science Foundation of China (NSFC) under Contracts Nos. 11975141, 11875115, 11625523, 11635010, 11735014, 11822506, 11835012, 11935015, 11935016, 11935018, 11961141012, 12022510, 12025502, 12035009, 12035013, 12061131003; the Chinese Academy of Sciences (CAS) Large-Scale Scientific Facility Program; Joint Large-Scale Scientific Facility Funds of the NSFC and CAS under Contracts Nos. U1732263, U1832207; CAS Key Research Program of Frontier Sciences under Contract No. QYZDJ-SSW-SLH040; 100 Talents Program of CAS; IN-PAC and Shanghai Key Laboratory for Particle Physics and Cosmology; ERC under Contract No. 758462; European Union Horizon 2020 research and innovation programme under Contract No. Marie Skłodowska-Curie grant agreement No 894790; German Research Foundation DFG under Contracts Nos. 443159800, Collaborative Research Center CRC 1044, FOR 2359, GRK 214; Istituto Nazionale di Fisica Nucleare, Italy; Ministry of Development of Turkey under Contract No. DPT2006K-120470; National Science and Technology fund; Olle Engkvist Foundation under Contract No. 200-0605; STFC (United Kingdom); The Knut and Alice Wallenberg Foundation (Sweden) under Contract No. 2016.0157; The Royal Society, UK under Contracts Nos. DH140054, DH160214; The Swedish Research Council; U. S. Department of Energy under Contracts Nos. DE-FG02-05ER41374, DE-SC-0012069.

-
- [1] M. Gell-Mann, Phys. Lett. 8, **214** (1964); G. Zweig, CERN Report **8182/TH.401**, 1 (1964).
[2] S. K. Choi *et al.* (Belle Collaboration), Phys. Rev. Lett. **91**, 262001 (2003).
[3] B. Aubert *et al.* (BABAR Collaboration), Phys. Rev. Lett. **95**, 142001 (2005).
[4] M. Ablikim *et al.* (BESIII Collaboration), Phys. Rev. Lett. **110**, 252001 (2013).
[5] Z. Q. Liu *et al.* (Belle Collaboration), Phys. Rev. Lett. **110**, 252002 (2013).
[6] S. L. Olsen, T. Skwarnicki, and D. Zieminska, Rev. Mod. Phys. **90**, 015003 (2018).
[7] N. Brambilla *et al.*, Phys. Rep. **873** (2020) 1-154.
[8] C. Z. Yuan *et al.* (Belle Collaboration), Phys. Rev. Lett. **99**, 182004 (2007).
[9] M. Ablikim *et al.* (BESIII Collaboration), Phys. Rev. Lett. **118**, 092001 (2017).
[10] B. Aubert *et al.* (BABAR Collaboration), Phys. Rev. Lett. **98**, 212001 (2007).
[11] X. L. Wang *et al.* (Belle Collaboration), Phys. Rev. Lett. **99**, 142002 (2007).
[12] M. Ablikim *et al.* (BESIII Collaboration), Phys. Rev. Lett. **118**, 092002 (2017).
[13] G. Pakhlova *et al.* (Belle Collaboration), Phys. Rev. Lett. **101**, 172001 (2008).
[14] S. Jia *et al.* (Belle Collaboration), Phys. Rev. D **100**, 111103(R) (2019); Phys. Rev. D **101**, 091101(R) (2020).
[15] J. P. Lees *et al.* (BABAR Collaboration), Phys. Rev. D **89**, 111103 (2014).
[16] M. Ablikim *et al.* (BESIII Collaboration), Phys. Rev. D **104**, 052012 (2021).
[17] Feng-Kun Guo, Christoph Hanhart, and Ulf-G. Meissner, Phys. Lett. B **665**, 26 (2008).
[18] C. F. Qiao, J. Phys. G **35**, 075008 (2008).
[19] L. Maiani *et al.*, Phys. Rev. D **89**, 114010 (2014).
[20] L. Antoniazzi *et al.* (E705 Collaboration), Phys. Rev. D **50**, 4258 (1994); V. Bhardwaj *et al.* (Belle Collaboration), Phys. Rev. Lett. **111**, 032001 (2013).
[21] M. Ablikim *et al.* (BESIII Collaboration), Phys. Rev. Lett. **115**, 011803 (2015).
[22] R. Aaij *et al.* (LHCb Collaboration), J. High Energ. Phys. **07**, 035 (2019).
[23] R. Aaij *et al.* (LHCb Collaboration), J. High Energ. Phys. **08**, 123 (2020); M. Ablikim *et al.* (BESIII Collaboration), Phys. Rev. D **103**, L091102 (2021); R. Aaij *et al.* (LHCb Collaboration), J. High Energ. Phys. **04**, 046 (2022).
[24] T. Barnes, S. Godfrey, and E. S. Swanson, Phys. Rev. D **72**, 054026 (2005).

- [25] M. Ablikim *et al.* (BESIII Collaboration), *Chin. Phys. C* **39**, 093001 (2015); *Chin. Phys. C* **40**, 063001 (2016); *Chin. Phys. C* **45**, 103001 (2021); *Phys. Rev. Lett.* **126**, 102001 (2021).
- [26] M. Ablikim *et al.* (BESIII Collaboration), *Nucl. Instrum. Methods Phys. Res., Sect. A* **614**, 345 (2010).
- [27] C. H. Yu *et al.*, Proceedings of IPAC2016, Busan, Korea, 2016, doi:10.18429/JACoW-IPAC2016-TUYA01.
- [28] X. Li *et al.*, *Radiat. Detect. Technol. Methods* **1**, 13 (2017); Y. X. Guo *et al.*, *Radiat. Detect. Technol. Methods* **1**, 15 (2017); P. Cao *et al.*, *Nucl. Instrum. Meth. A* **953**, 163053 (2020).
- [29] S. Agostinelli *et al.* (GEANT4 Collaboration), *Nucl. Instrum. Methods A* **506**, 250 (2003).
- [30] D. J. Lange, *Nucl. Instrum. Meth. A* **462**, 152 (2001); R. G. Ping, *Chin. Phys. C* **32**, 599 (2008).
- [31] S. Jadach, B. F. L. Ward, and Z. Was, *Comput. Phys. Commun.* **130**, 260 (2000).
- [32] E. Richter-Was, *Phys. Lett. B* **303**, 163 (1993); P. Golonka, and Z. Was, *Eur. Phys. J. C* **45**, 97 (2006).
- [33] M. Ablikim *et al.* (BESIII Collaboration), *Phys. Rev. Lett.* **104**, 132002 (2010).
- [34] In this Letter, definitions of $M(\pi^+\pi^-J/\psi) \equiv M(\pi^+\pi^-\ell^+\ell^-) - M(\ell^+\ell^-) + m(J/\psi)$ and $M(\gamma_H J/\psi) \equiv M(\gamma_H \ell^+\ell^-) - M(\ell^+\ell^-) + m(J/\psi)$ are used to partly cancel the mass resolution of the lepton pair. Here $m(J/\psi)$ and $m[\psi(2S)]$ are the nominal masses of J/ψ and $\psi(2S)$, respectively [41].
- [35] M. Ablikim *et al.* (BESIII Collaboration), *Phys. Rev. D* **94**, 032009 (2016).
- [36] M. Ablikim *et al.* (BESIII Collaboration), *Phys. Rev. D* **93**, 011102(R) (2016); *Phys. Rev. Lett.* **122**, 232002 (2019).
- [37] See the Supplemental Material at [PhysRevLett.129.102003](https://arxiv.org/abs/1910.10203) for the numerical results for $\sigma[e^+e^- \rightarrow \pi^+\pi^-\psi_2(3823)] \times \mathcal{B}[\psi_2(3823) \rightarrow \gamma\chi_{c1}]$.
- [38] M. Ablikim *et al.* (BESIII Collaboration), *Phys. Rev. D* **104**, 092001 (2021).
- [39] M. Ablikim *et al.* (BESIII Collaboration), *Phys. Rev. Lett.* **112**, 092001 (2014).
- [40] M. Ablikim *et al.* (BESIII Collaboration), *Phys. Rev. D* **87**, 012002 (2013).
- [41] R. L. Workman *et al.* (Particle Data Group), *Prog. Theor. Exp. Phys.* **2022**, 083C01 (2022).
- [42] M. Ablikim *et al.* (BESIII Collaboration), *Phys. Rev. D* **100**, 032005 (2019).
- [43] C. F. Qiao, F. Yuan, and K. T. Chao, *Phys. Rev. D* **55**, 4001 (1997).

APPENDIX

I. NUMERICAL RESULTS OF

$$\sigma[e^+e^- \rightarrow \pi^+\pi^-\psi_2(3823)] \cdot \mathcal{B}[\psi_2(3823) \rightarrow \gamma\chi_{c1}]$$

TABLE II. The measured cross section $\sigma[e^+e^- \rightarrow \pi^+\pi^-\psi_2(3823)]$ times the branching ratio $\mathcal{B}[\psi_2(3823) \rightarrow \gamma\chi_{c1}]$ at different c.m. energies. Here the uncertainties are statistical only.

\sqrt{s} (GeV)	$\mathcal{L}_{\text{int}}(\text{pb}^{-1})$	N^{sig}	ϵ	$1 + \delta$	$\sigma \cdot \mathcal{B}$ (pb)
4.2263	1056.4	$1.7^{+2.5}_{-1.7}$	0.311	0.737	$0.17^{+0.28}_{-0.18}$
4.2580	828.4	$1.2^{+2.1}_{-1.3}$	0.336	0.741	$0.15^{+0.25}_{-0.16}$
4.2879	502.4	$0.7^{+1.8}_{-1.0}$	0.334	0.743	$0.13^{+0.35}_{-0.19}$
4.3121	501.2	$0.6^{+1.9}_{-1.0}$	0.343	0.743	$0.11^{+0.36}_{-0.20}$
4.3374	505.0	$3.4^{+2.5}_{-1.8}$	0.356	0.742	$0.63^{+0.47}_{-0.34}$
4.3583	543.9	$6.7^{+3.2}_{-2.5}$	0.357	0.744	$1.13^{+0.54}_{-0.42}$
4.3774	522.7	$8.3^{+3.7}_{-3.0}$	0.338	0.750	$1.54^{+0.68}_{-0.55}$
4.3965	507.8	$12.3^{+4.2}_{-3.5}$	0.318	0.767	$2.42^{+0.83}_{-0.69}$
4.4156	1043.9	$14.2^{+5.2}_{-4.5}$	0.310	0.798	$1.35^{+0.49}_{-0.42}$
4.4362	569.9	$12.5^{+4.3}_{-3.6}$	0.323	0.841	$1.98^{+0.67}_{-0.56}$
4.4671	111.1	$5.3^{+2.9}_{-2.2}$	0.332	0.910	$3.85^{+2.09}_{-1.60}$
4.5271	112.1	$0.0^{+1.6}_{-0.0}$	0.320	1.017	$0.00^{+1.07}_{-0.00}$
4.5745	48.9	$2.0^{+1.8}_{-1.1}$	0.307	1.053	$3.02^{+2.82}_{-1.77}$
4.5995	586.9	$2.1^{+2.5}_{-1.7}$	0.318	1.014	$0.27^{+0.32}_{-0.22}$
4.6120	102.5	$1.5^{+1.9}_{-1.2}$	0.328	0.960	$1.12^{+1.45}_{-0.93}$
4.6278	511.1	$7.0^{+3.8}_{-3.0}$	0.348	0.860	$1.12^{+0.60}_{-0.48}$
4.6408	541.4	$10.0^{+3.9}_{-3.2}$	0.371	0.783	$1.56^{+0.60}_{-0.50}$
4.6613	523.6	$14.3^{+4.5}_{-3.8}$	0.384	0.796	$2.18^{+0.69}_{-0.58}$
4.6811	1631.7	$22.2^{+6.0}_{-5.2}$	0.364	0.943	$0.97^{+0.26}_{-0.23}$
4.6984	526.2	$6.2^{+3.5}_{-2.8}$	0.340	1.042	$0.81^{+0.46}_{-0.37}$

II. SYSTEMATIC ERROR OF RESONANCE PARAMETERS

III. RESULTS OF $\mathcal{B}[\psi_2(3823) \rightarrow \gamma\chi_{c2}]$

For the $\psi_2(3823) \rightarrow \gamma\chi_{c2}$ decay, we study the $M(\gamma_H J/\psi)$ distribution by requiring $3.815 < M^{\text{recoil}}(\pi^+\pi^-) < 3.835 \text{ GeV}/c^2$ to select $\psi_2(3823)$ signal candidates. In order to estimate non- $\psi_2(3823)$ background, we also define a sideband region as $3.74 < M^{\text{recoil}}(\pi^+\pi^-) < 3.78 \text{ GeV}/c^2$. Figure 3 shows the $M(\gamma_H J/\psi)$ distribution, where no significant χ_{c2} signal is seen. A fit with χ_{c1} and χ_{c2} signal shapes determined from MC simulation as the signal PDF, and a second-order polynomial as the background is used to extract the relative decay rate of $R = \frac{\mathcal{B}[\psi_2(3823) \rightarrow \gamma\chi_{c2}]}{\mathcal{B}[\psi_2(3823) \rightarrow \gamma\chi_{c1}]} = 0.33 \pm 0.12$. Since the χ_{c2} signal is not significant (the statistical significance is only 2.0σ), an upper limit of $R < 0.51$ at the 90% C.L. is given, taking into account the systematic uncertainty.

TABLE III. The systematic uncertainties for the resonance parameters. $M[R_i]$ and $\Gamma_{\text{tot}}[R_i]$ represent the mass (in MeV/c^2) and total width (in MeV) of resonance R_i , respectively; $\Gamma_{e^+e^-} \mathcal{B}_1^{R_i} \mathcal{B}_2$ is the product of the e^+e^- partial width (in eV/c^2) and branching fraction of $R_i \rightarrow \pi^+\pi^-\psi_2(3823) \rightarrow \pi^+\pi^-\gamma\chi_{c1}$ ($i = 1, 2$). The parameter ϕ (in degrees) is the relative phase between the two resonances, and the values in the brackets are the corresponding systematic uncertainties for the second solution of the two-BW fit.

Parameters	\sqrt{s}	$\sigma \cdot \mathcal{B}$	Fit model	Sum
$M[R_1]$	3.9	–	2.2	4.5
$\Gamma_{\text{tot}}[R_1]$	1.6	–	1.6	2.3
$\Gamma_{e^+e^-} \mathcal{B}_1^{R_1} \mathcal{B}_2$	0.01 (0.01)	0.03 (0.03)	0.01 (0.01)	0.03 (0.03)
$M[R_2]$	0.7	–	0.4	0.8
$\Gamma_{\text{tot}}[R_2]$	0.4	–	4.1	4.1
$\Gamma_{e^+e^-} \mathcal{B}_1^{R_2} \mathcal{B}_2$	0.01 (0.01)	0.02 (0.01)	0.01 (0.01)	0.02 (0.01)
ϕ	0.3 (1.8)	–	3.2 (5.4)	3.2 (5.7)
$M[R]$	3.2	–	1.3	3.5
$\Gamma_{\text{tot}}[R]$	1.7	–	12.2	12.3
$\Gamma_{e^+e^-} \mathcal{B}_1^R \mathcal{B}_2$	0.01	0.05	0.02	0.05

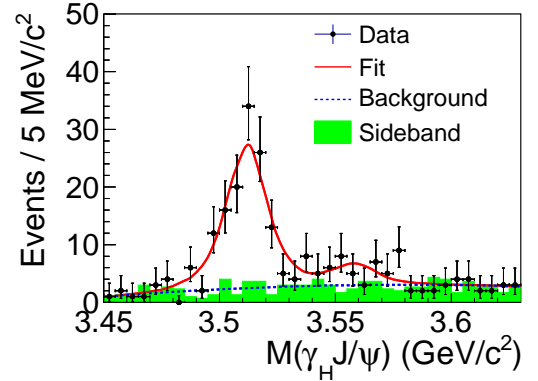


FIG. 3. Result of the fit to the $M(\gamma_H J/\psi)$ distribution for the events in the $\psi_2(3823)$ signal region ($3.815 < M^{\text{recoil}}(\pi^+\pi^-) < 3.835 \text{ GeV}/c^2$). Dots with error bars are data, the red solid curve is the total fit, the blue dashed curve is background, and the green shaded histogram is the background estimated from $\psi_2(3823)$ sideband events.

IV. SCATTERING ANGLE DISTRIBUTION

The $\pi^+\pi^-$ system in the $e^+e^- \rightarrow \pi^+\pi^-\psi_2(3823)$ process is expected to be dominated by S -wave, such as $f_0(500)$. According to spin-parity conservation, the orbital angular momentum L between $\pi^+\pi^-$ and $\psi_2(3823)$ is therefore 2. With helicity amplitude calculations, the scattering angle distribution of $\psi_2(3823)$ is $(1 + \cos^2\theta)$, where θ is the polar angle of $\psi_2(3823)$ in the e^+e^- c.m. frame. Figure 4 shows the $\cos\theta$ distribution of the selected $e^+e^- \rightarrow \pi^+\pi^-\psi_2(3823)$ signal candidates after efficiency correction. We perform fits to the angular distribution with an $L = 0$ PDF (flat) and an $L = 2$ PDF ($1 + \alpha \cos^2\theta$, where $\alpha = 1.3 \pm 0.8$ is

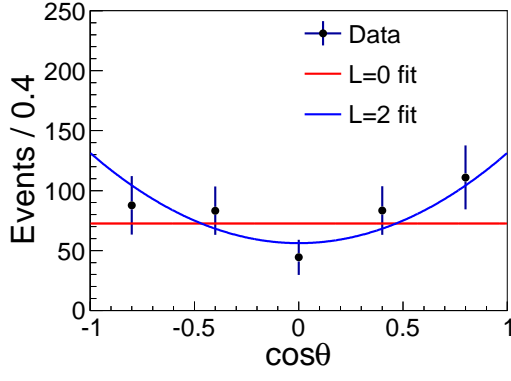


FIG. 4. Scattering angle distribution for $\psi_2(3823)$ events in e^+e^- CM frame (after efficiency correction). Dots with error bars are data, the red and blue curves are from the $L = 0$ and $L = 2$ fits, respectively.

obtained from the fit). A χ^2 -test for the $L = 2$ fit yields $\chi^2/ndf = 2.3/3 = 0.8$, which is better than that of the $L = 0$ fit ($\chi^2/ndf = 6.8/4 = 1.7$).